Exoplanet Observing and Characterisation

Tomas James

Abstract

For this project, the transiting extrasolar planets WASP-22 b, WASP-78 b and HATS-5 b were chosen to be observed using LCOGT telescopes in the Southern Hemisphere. The data obtained from these observations was then analysed using aperture photometry in GAIA in order to plot lightcurves for each dataset. The lightcurves produced did not show any visible transits, so datasets of the extrasolar planets HAT-P-25, Qatar-1b and WASP-12b (provided by project supervisor Dr. E. L. Gomez) were analysed in replacement. These lightcurves were then used to estimate upper limits for the radius of each exoplanet. Furthermore the Exoplanetary Transit Pixelisation Model developed by Addison, Durrance, and Schwieterman (2010) was adapted in order to computationally model the transits leading to further estimates of exoplanetary radius. These results were then compared with each other, as well as the known published values.

Contents

I. Introduction

The discovery of the first extrasolar planet by Wolszszan and Frail (1992) introduced a field into astronomical research that is now one of the most exciting and fast moving fields in modern astrophysics. Subsequent detections, such as the first main-sequence extrasolar planet by Mayor and Queloz (1995) continue to reveal a more diverse and rich spectrum of exoplanets. More than 20 years on from these detections, the Extrasolar Planets Encyclopaedia (2014) records 1854 [1] extrasolar planets that have been discovered using a variety of detection methods utilising both ground and satellite based telescopes in a multitude of collaborative missions. These vary from discovering new exoplanets to actively searching for Earth analogs that could, under the right circumstances, harbour life.

I. Extrasolar Planets

Extrasolar planets - or exoplanets - are planetary objects orbiting stars outside of the Solar System. The Solar System itself is the subject of intense study, largely because of its relative ease to study. In comparison, exoplanetary detection is much harder, as Kepler estimates the closest Earth-like planet is still 9ly from Earth [reference]. Statistics place the number of potential planetary systems at 400 billion [reference], but relatively little is known as to their analogy to the Solar System. Is the Solar System a common planetary system or is it a much more peculiar system, one of chance and luck rather than mean statistics?

Since the detections made by Wolszszan and Frail and Mayor and Queloz a multitude of dedicated projects have been launched with the primary aim of detecting and characterising exoplanets. These vary from ground-based telescopes such as WASP and HAT to spaced-based telescopes such as Kepler and CoRoT. Uniquely these missions observe a wide distribution of exoplanets, effectively allowing the formation and evolution of planetary systems to be studied.

One of the most prominent and substantial of these missions is NASA's Kepler mission. Launched on March 7th 2009, the primary objective of Kepler is to detect exoplanets of Earth size that reside in or close to the habitable zone of their parent stars. A key advantage of Kepler is that it orbits the Sun and so its observations are not constrained by Earth's atmosphere. Shortly after launch, Kepler encountered mechanical failure that limited its ability to hunt for Earth sized planets. In 2014, the K2 mission - a modified form of Kepler's initial mission to take into account the mechanical failures - was greenlit such that Kepler now searches primarily for habitable planets orbiting red-dwarf Stars along with potential supernova events and star forming regions. In spite of this Kepler has still discovered over 1000 confirmed exoplanets and is synonymous with the hunt for extrasolar planets, having discovered a large portion of the current dataset [insert some more rigorous statistics].

II. Detection Methods

Extrasolar planet detection methods are divided into two classes: direct and indirect detections. A direct detection uses data that explicitly shows the presence of an extrasolar planet. An indirect detection uses effects that an extrasolar planet has on its parent star to infer the planet's existence. To date there are 5 well established detection methods. These are discussed below.

Transiting

When an exoplanet passes across the line of sight between the observer and a star, a dip in the total luminosity of the system is observed owing to the exoplanet blocking a portion of the star's flux from the observer. By plotting the total flux received as a function of time the presence of an exoplanet can be inferred if a dip in the total flux received is observed. Furthermore the dip in the total flux allows the calculation of the size of the exoplanet, as the amount of flux blocked is proportional to the exoplanet radius as described by equation 1 (Charbonneau et al. 2007). An example of this effect can be seen in Figure 1.

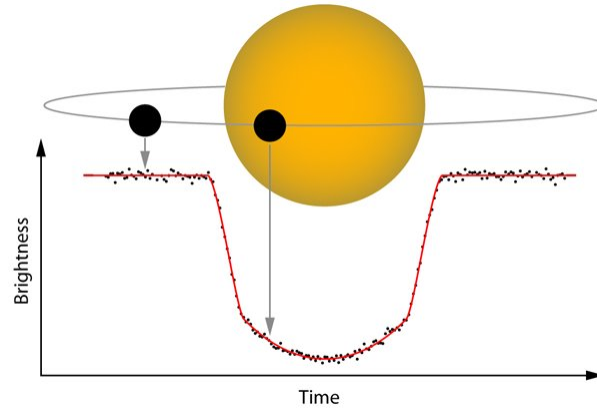
[1] As of Friday 12th December 2014

Figure 1: *An example showing how the presence of an exoplanet moving across a star results in a reduction in the observed flux, as evidenced by the visible trough. (NASA Exoplanet Archive 2010)*

$$\frac{\Delta F}{F} = \frac{R_{exo}^2}{R_{star}^2} \tag{1}$$

In equation 1 ΔF is the flux blocked due to the exoplanet, F is the observed off transit flux, R_{exo} is the radius of the exoplanet and R_{star} is the radius of the star being transitted.

This method has various limitations however. This method is biased towards finding exoplanets with large radii and small orbital periods as they block more of the stars flux incident upon the observer more often. This allows more reliable estimates of parameters like exoplanetary radius to be determined. Another limitation is that exoplanets with orbital inclinations close to $90°$ cannot be detected as they do not pass in front of their host star relative to the observer.

Moreover, any partially opaque object passing infront of a star will have the effect of blocking a portion of the star's total flux. Morton and Johnson (2011) estimated that this is a rare occurence, with the false positive probability (FPP)[2] being estimated at $< 10\%$ for almost 90% of candidates being observed by the Kepler mission.

Radial Velocity

The existence of an exoplanetary companion orbiting a host star alters the system's centre of mass causing both the exoplanet and host star to orbit about it. As a direct result of this the radial velocity of the star changes over time, peaking at a maximum when the star is moving directly toward, or away from, the observer. Conversely the radial velocity of the star is at a minimum when the star moves normal to the observer's line of sight. This is demonstrated in Figure 2.

---

[2]The FPP is the probability that the exoplanet detected is a false positive, or an astronomical object passing between the telescope and the star, therefore acting as an erroneous detection.
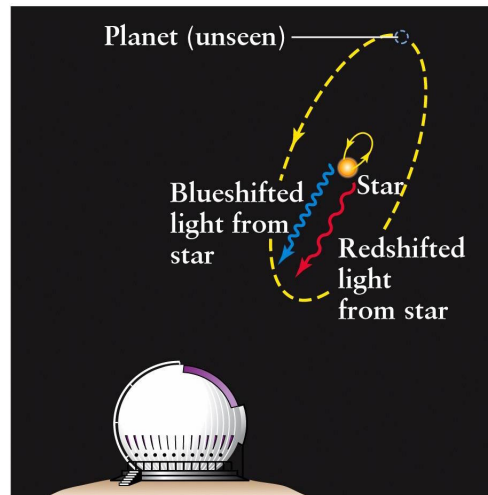
Figure 2: *An example showing how the presence of a hidden exoplanet induces a change in the centre of mass of the planetary system, therefore altering the centre of orbit of each of the system's orbiting companions. This can be detected by the resulting Doppler shift of the host star's spectral lines. (Townsend 2013)*

This variation is detected by observing the Doppler shift of the stars spectral lines. Whilst the star is moving towards the observer a decrease in the wavelength of the spectral lines is observed. When it is moving away from the observer an increase in the wavelength of the spectral lines is observed. No change is observed when the star is moving normal to the observer's line of sight.

This detection method is heavily biased towards large exoplanets orbiting less massive stars with small orbital periods, owing to the larger perturbation observed in the host stars orbit. However as Udry and Santos (2007) state, the spectroscopic signature can only yield orbital parameters and a minimum mass as the orbital inclination remains unknown. An example of this bias is the inherent abundance of 'hot-Jupiters' in the current data. Hot Jupiters are exoplanets close to the mass of Jupiter that orbit their host star at very small semi-major axes. For example, Sahu et al. (2006) surveyed multiple Jovian mass exoplanets in the SWEEPS field and found that the orbital periods varied from 0.541-2.965 days. These combinations produce a perturbation detectable using the radial-velocity method, accounting for the potentially over-sampled number of Jovian class exoplanets detected in surveys to date.

A common source of error using the radial velocity method relates to the expansion and contraction of the star itself. This produces a very similar spectroscopic signature that would be expected to be observed were the star's orbit to be perturbed by an exoplanet.

Direct Imaging

Direct imaging detections utilise the thermal emission of an extrasolar planet to detect the planet as a source of infrared radiation in an image taken in the infrared.

The method of direct imaging is heavily biased towards large, hot planets that are seperated by a large distance from their host star. This highlights a major disadvantage that direct imaging has: exoplanets lying close to a large, luminous star will be hidden owing to the large infrared luminosity difference between the two objects.

Typically this limitation is solved by the attachment of a coronograph which blanks out the host star to avoid complications relating to its presence in the image. This is especially useful for solving problems related to the large infrared luminosity difference between a star and planet. This allows the use of longer exposure times, aiding in the potential discovery of cool exoplanets.

Microlensing

Gravitational microlensing is an effect observed in the presense of strong gravitational fields. Specifically when light interacts with a strong gravitational field it bends and undergoes magnification (Einstein 1936). As stated by Sumi et al. (2011), 'in a gravitational microlensing event, a foreground lens object is detected as a result of the characteristic magnification of a background source star as it passes behind the gravitational field of the lens'. On smaller scales an increase in brightness is observed rather than magnification.

Applying this to exoplanetary detection, light from a star beyond an exoplanetary system in the observer's line of sight (the background source star) is lensed and magnified by the strong gravitational field of the system itself (the lens star). If an exoplanet is orbiting the lens star, an increase in the magnification or brightness is observed for a small duration. This anomaly can lead to the calculation of the exoplanet's mass, as well as its semi-major axis.

Projects such as OGLE are dedicated microlensing surveys that detect exoplanets using this method. This method does however require precise alignment between background and lens stars in order for any lensing to occur. Lensing events are not periodic and often rely on the random alignment of a lens and background star. As a result of this the number of detected exoplanets according to Extrasolar Planets Encyclopaedia (2014) using the microlensing method is comparitively small (34) in relation to that of the radial-velocity (583) or transit methods (1163).

Pulsar Timing

Pulsar timing detections rely on the regular, periodic bursts of radio emission from an ultradense, rapidly rotating neutron star, or a pulsar.

This radio emission - owing to its stability and reliability - can be used to track the orbital period of the star. If a planetary companion is orbiting the pulsar then small orbital perturbations are to be expected owing to the orbit of the system about a common centre of mass. This results in periodic anomalies in the detection of the emitted radio signal as the star moves around the centre of mass of the system. Tracking these anomalies allows the period of the star to be determined and crucially, the mass and orbital parameters of the exoplanet as well.

The reliability and accuracy of the pulsar timing method allows much smaller exoplanets to be detected. The first discovered exoplanet was found orbiting the pulsar PSR1257+12 by Wolszszan and Frail in 1992. According to the Extrasolar Planets Encyclopaedia (2014) however only 18 exoplanets have been detected using this method since 1992, indicating that exoplanets orbiting pulsars are rare occurences.

III.   Statistical Properties of Known Exoplanets

To better understand the orbital behaviour of exoplanets, along with their calculated properties, graphs that could potentially reveal trends were plotted. This was achieved by using the Extrasolar Planets Encyclopaedia (2014) to download[3] data on all detected exoplanets. A Python script was written to process this data with the primary aim of reducing it the required graphs.

---

[3]The last download of this data was 12th December 2014
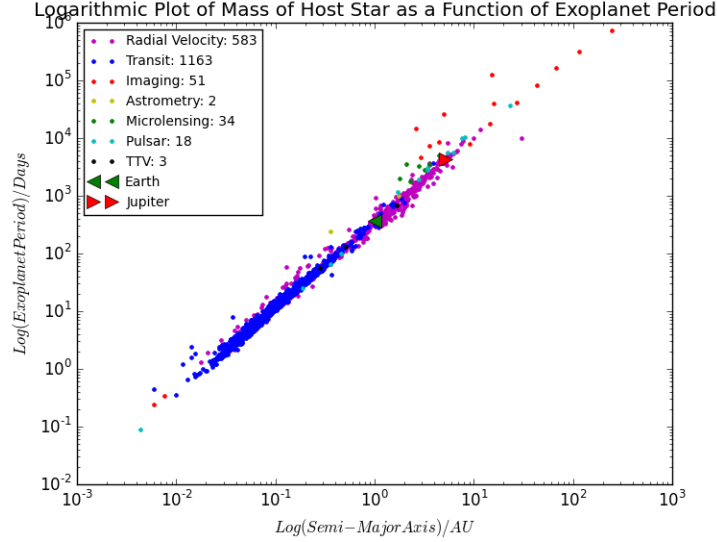
Period and Semi-Major Axis

Figure 3: *A loglog plot showing the relationship between an exoplanet's period and its semi-major axis.*

As can be seen in Figure 3 the loglog plot of orbital period vs semi-major axis produces a very well defined and characteristic straight line. Kepler's 3rd Law relates period and semi-major axis as defined in Haswell (2010) by equation 2.

$$T^2 = \frac{4\pi^2}{G(M_{star} + M_{exo})} a^3 \tag{2}$$

In this instance T is the orbital period, *a* is the semi-major axis, *G* is the universal gravitational constant, M_{star} is the mass of the host star and M_{exo} is the mass of the exoplanet. Given that orbital systems are bound by Kepler's Laws (the Jupiter and Earth points confirm that this is the case for those 2 Solar System planets) the shape of the graph is to be expected, however Kepler's 3rd law uses the mass of the body being orbited as a proportionality constant as illustrated. In this case, this constant is the mass of the host star. This means that whilst the shape of the graph is correct, a number of distinct lines is to be expected due to the varying masses of host stars. The existence of one primary line points to there being limitations on the mass of the host star, however a more likely explanation is that Kepler, having detecting the majority of known exoplanets, has introduced bias into the dataset owing to it primarily looking for Solar System analogues. The erroneous Kepler data points that do not appear to fit this trend could be detections during the adapted K2 mission. Interestingly a number of points lie off this main line in Figure 3, even factoring for the potential biases. Regrettably the Extrasolar Planets Encyclopaedia (2014) does not include error estimations for all exoplanet entries, meaning firm conclusions about why these points lie off of the main sequence cannot be drawn without speculation.

Figure 3 also allows analysis of the sensitivity of each detection method. For example the exoplanet with the fastest orbital period and smallest semi-major axis was detected using the pulsar timing method, whilst the exoplanet with the slowest period and largest semi-major axis was detected using the direct imaging method. Direct imaging does however detect exoplanets across the most diverse range of periods and semi-major axes of those detection methods considered, ranging from the second-smallest semi-major axis to the largest.

Furthermore Figure 3 shows that nearly all exoplanets detected using the transit method orbit at <1 AU with orbital periods <365 days. This shows graphically the bias towards small semi-major axis and short period. Very few exoplanets are observed with orbital characteristics in excess of Jupiter (a semi-major axis >5.2 AU and period >4332 days). The

aforementioned bias and minimal detections using methods that are capable of detecting exoplanets with larger semi-major axes and longer period mean the existence of exoplanets at these orbital parameters cannot be dismissed.
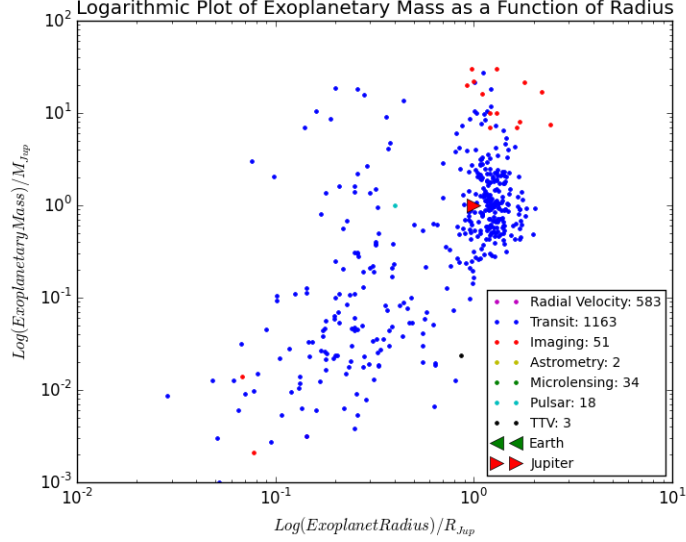
Mass-Radius Relationship

Figure 4: *A loglog plot showing the relationship between an exoplanet's mass and its radius.*

Considering Figure 4, a general trend is observed showing that mass is correlated with radius. Mass and radius are linked through equation 3.

$$m = \frac{4}{3}\pi R^3 \rho \tag{3}$$

where m is the planetary mass, R is the planetary radius and ρ is the planetary density. If equation 3 describes the profile shown in Figure 4, then the deviation from constant positive correlation is due to ρ varying (i.e. ρ is not constant across all exoplanets). This behaviour is observed in the Solar System, as the calculated densities vary for all Solar System planets. For density to be calculated however both the precise mass and radius need to be known. As a result both the radial velocity and transit detection methods need be used in order to determine these quanitities reliably.

Interestingly a grouping of data points exists close the 1 R_{Jup} marker, indicating a large number of exoplanets having a radius close to this value. Jupiter like exoplanets are not uncommon. As stated by Udry and Santos (2007), the limitations in observation techniques lend themselves to detecting Jupiter like planets. Whilst this grouping has a narrow spread of radii close to the 1 R_{Jup}, its associated mass is spread over a much larger range, indicating non-uniform density.

Figure 4 also highlights how dominant the transit detection method is, having twice the number of confirmed detections than all other detection methods combined. It also confirms that the transit method can detect exoplanets across the largest mass range. Both Figures 3 and 4 follow confirmed mathematical trends and show that the Solar System isn't an anomolous planetary system.

IV. LCOGT Observatories

Observations were limited to LCOGT sites in the Southern Hemisphere owing to a greater number of available telescopes. These sites are listed in Table 1.

Observatory	Latitude (Deg)	Longitude (Deg)
Cerro Tololo	30° 10' 2.64"S	70° 48' 17.28"W
Sutherland	32° 22' 48"S	20° 48' 36"E
Siding Spring	31° 16' 23.88"S	149° 4' 15.6"E

Table 1: *A table showing the observatories housing LCOGT telescopes that were used for data collection during this project* (LCOGT Observatory Sites *2014).*

As all of the sites in Table 1 house 1.0m Ritchey-Chretien Cassegrain telescopes, it was this variety of instrument that was used to collect data. Of all of these sites however, Siding Spring is the only telescope to currently have both a 2.0m and 1.0m Ritchey-Chretien variant.

Each 1.0m telescope allows for the selection of 2 different sensors, along with a range of filters (*LCOGT 1-meter Telescope Specifications* 2014).

- SBIG STX-16803, FOV 16x16 arcmin

- Sinistro Fairchild CCD-486 BI, FOV 27x27 arcmin

Whilst it would have been preferable to use one sensor across all observations and observatories, not all observatories in the Southern Hemisphere use the same sensor. Both Sutherland and Siding Spring operate using the SBIG sensor whilst Cerro Tololo uses the Sinistro sensor.

II. Observed Exoplanets

Observations were required to be obtained during the time frame October 2014 - December 2014. To determine which exoplanets were visible during this period, the STARALT tool (Sorensen, Azzaro, and Méndez 2002) was used in conjuction with the Exoplanet Transit Database (Paddany, Brat, and Pejcha 2014). Only transiting exoplanets were considered for this project as equipment required for other detection methods was not available at the observatories used.

I. Selection Criteria

Once the number of visible sources was determined, the number of those sources that were undergoing visible transits during the required time period was determined using the ETD's Transit Prediction function. These were crossreferenced using the STARALT function STARMULT, which produces an optimal observing date for a given source based on the observatory coordinates in Table 1 and stipulation that observations must occur above an altitude of 30° above the horizonfootnoteThe airmass below this altitude would have rendered any observations highly prone to errors from atmospheric effects. The candidates for observation can be seen in Table 2.

Exoplanet	RA	Dec	Date
WASP-22 b	03h 31m 16.3s	-23° 49' 11"	09/11/2014
WASP-78 b	04h 15m 02.0s	-22° 06' 59.1"	30/11/2014
HATS-5 b	04h 28m 53.47s	-21° 28' 54.0"	01/12/2014

Table 2: *A table showing the exoplanets to be observed in this project along with the proposed date of observation and the coordinates, in RA/Dec, of each source (Paddany, Brat, and Pejcha 2014).*

The data from these observations was regrettably unusable. Whilst steps were taken to minimise the possibility of observation limiting effects, it was suspected that bad weather or atmospheric anomalies contributed in masking any transit the data may have captured.

III. Methodology

I. Data Collection

In order to determine the best exposure times for each candidate, initial test exposures were assigned to each system - these test exposures varied in 10s integration time increments from 30s - 90s. The resulting files were then assessed manually to determine the quality of the data and subsequently the best integration time.

This process determined that 90s exposures for all systems generated the best quality data. A longer exposure time is preferable in order to maximise the SNR[4].

For an exoplanet to be characterised it is necessary to observe the system as many times as possible over the duration of the transit. A baseline flux outside of the transit is also needed in order for the transit itself to be visible, so exposures were started 15 minutes before the estimated transit start (i.e. 15 minutes before the planet first occults the host star) and concluded 15 minutes after the transit ended. The optimum number of exposures was calculated using equation 4.

$$N_e = \frac{D_{transit} + 2t_{window}}{t_e + t_{read}} \tag{4}$$

In equation 4, N_e is the maximum number of exposures, $D_{transit}$ is the transit duration in seconds, t_{window} is the time between observations beginning and transit beginning, t_e is the exposure time in seconds and t_{read} is the necessary readout time for the telescope in use. In this case, $t_{window} = 900s$ and $t_{read} = 15s$.

Whilst N_e is the theoretical maximum number of exposures possible, this was reduced by a relative number of exposures to allow the telescope in use to prepare for the next exposure in ample time.

LCOGT's online scheduler was used to insert the observation requests into the observation queue.

II. Data Analysis

LCOGT systems use data reduction pipelines based upon the ORAC-DR infrastructure developed by Jenness et al. (2014) for UKIRT and JCMT initiatives. The pipeline reducing data from the LCOGT system runs multiple independent recipes for bad-pixel masking, bias subtraction, flat field correction and WCS fitting (*LCOGT Data Pipeline* 2012).

The resulting pipeline reduced and corrected data was then downloaded from the LCOGT Data Archive and analysed. In the case of this project the primary form of data analysis comprised of aperture photometry using the GAIA package, available as part of the Starlink Project (Draper et al. 2014).

III. Aperture Photometry

Photometry is a technique for measuring an object's incident radiation flux. Measurements made with this method can be used to calculate that object's luminosity and/or magnitude.

To perform aperture photometry using GAIA, the data (in the form a .FITS file) was loaded and a circular aperture was placed over the object to be analysed. Initially GAIA sums all object data counts within the aperture. In this analyses a seperate, independent circular background aperture was used in order to capture a sky area. This was used as it eliminated any stray flux from the object that may contaminate the background count. The incident flux is then calculated by $F_i = F_{o+b} - F_b$ where F_i is the incident flux from the object alone, F_{o+b} is the flux incident from the object and background and F_b is the flux from the background alone.

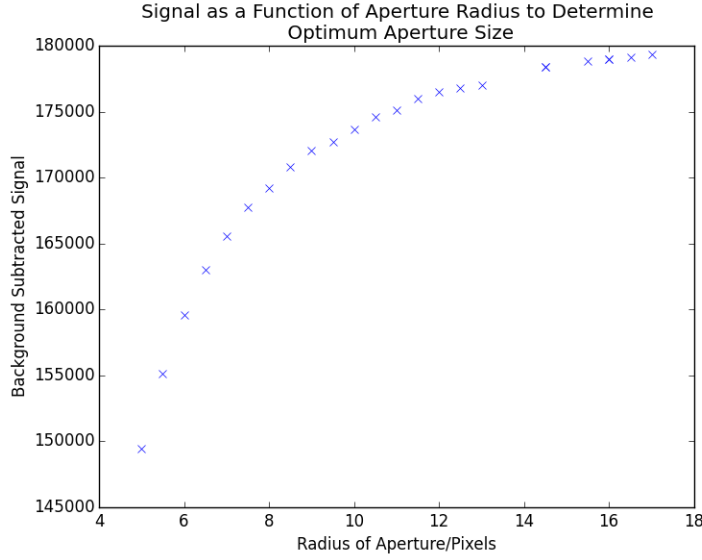[4] $SNR \propto \sqrt{t}$ where t is the integration time

Figure 5: *An example of how the optimum aperture size was determined by observing how the background subtracted signal varies with aperture size. The point at which the gradient of the curve becomes constant - in this instance at the 12 pixel point - is the optimum aperture size.*

The required aperture size varies with the luminosity of the star in question, along with its radius. An aperture that is too small will not capture all of the star's flux and indeed an aperture that is too large will collect a larger portion of the background flux. To determine the optimum aperture size it was decided to perform aperture photometry on the star with a variety of different aperture sizes. The resulting background subtracted count was then plotted against the aperture size to assess how the count varied with aperture radius. An example for Qatar-1 b, provided by project supervisor Dr. E Gomez, is seen in Figure 5.

As the aperture size increases, so does the measured count inside of the aperture. When all of the star's flux has been measured, any further increase in aperture size will detect a uniform, constant background leading to a constant increase in the count. This is manifested graphically by a constant gradient. The point at which the graph plateaus is the optimum aperture size.

For a transit to be reliably characterised differential aperture photometry is performed in addition to the above using equation 5.

$$S = \frac{F_i}{F_c - F_b} \tag{5}$$

In equation 5, S is the calibrated flux, F_i is the incident flux as defined earlier, F_c is the calibration star flux and F_b is the background flux.

This essentially calibrates the flux from the object of interest against another object of similar brightness in the field of view. Providing that the calibration star has constant luminosity (and therefore constant flux) this normalises the count in order to account for any atmospheric effects between frames. In order to determine whether a calibration star has any variability the flux ratio was calculated using $F_{ratio} = \frac{F_1 - F_b}{F_2 - F_b}$ where F_1 and F_2 are the incident fluxes from 2 calibration stars. This was then plotted as a function of time. A nonvariable star will show random Poisson fluctuations in the count owing to photons obeying Poisson statistics, but these fluctuations should be around a constant mean value. If there is any deviation from this (i.e. F_{ratio} is not constant) then the variable star is discounted as a calibration star. For reliability this is performed with as many different calibration stars as the field of view allows. This project focused on obtaining at least 5 lightcurves using 5 different calibration stars.

This procedure is repeated across an even number of exposures, evenly distributed across the transit and, importantly,

about its transit centre. A Python script was then written to plot S as a function of time, thereby producing lightcurves for each calibration star.

IV. Modelling the Transit with the Exoplanet Pixelisation Transit Model

The Exoplanet Pixelisation Transit Model is a theoretical model developed by Addison, Durrance, and Schwieterman (2010) to fit an optimised, model lightcurve to an observed lightcurve. This splits an exoplanet into a 2D grid of pixels and determines the distance between each pixel to the centre of the star in a given time step (d_{pix}). If this distance is less than or equal to the stellar radius (R_{star}) then the pixel considered lies infront of the star relative to the observer's line of sight. This distance can be calculated using equation 6.

$$d_{pix} = \sqrt{(X_{pos} + x_{pix})^2 + (Y_{pos} + y_{pix})^2} \tag{6}$$

Essentially this remains a classical Pythagorean triangle problem, repeated for each pixel in the exoplanet. X_{pos} represents the distance from the centre of the transit to the exoplanet perpendicular to the line of sight (the centre of the star was assumed to be the centre of the transit). x_{pix} is the distance from the centre of the exoplanet to the pixel considered in the x-plane. These definitions hold similarly for both Y_{pos} and y_{pix} only in the y-plane.

Integrating over the observation period allows the exoplanet to move across the body of the star. Equation 7 is then used to determined the amount of flux blocked by the exoplanet (F_b).

$$F_b = \Delta\Omega_{pix} \sum_{pixels} I_0 \left[1 - \mu \left(1 - \sqrt{1 - \left(\frac{d_{pix}}{R_{star}} \right)^2} \right) \right] \tag{7}$$

μ is the limb darkening coefficient for the star considered, I_0 is the central band intensity of the star and $\Delta\Omega_{pix}$ is the solid angle per pixel. This is then summed over each pixel lying within R_{star} in order to account for all pixel blocking contributions. Crucially equation 7 uses μ to account for the non-uniform flux across the body of the star. For example the star's limb is less bright than the star's body, as the optical depth increases towards the centre of the star. As a result the flux blocked in the limb will be inherently less than the flux blocked in the body of the star even if the number of pixels lying infront of each is the same. The effective temperature of the host star for each system was known, which allowed the value of μ to be found using the tables in Van Hamme (1993).

The solid angle term, $\Delta\Omega_{pix}$, was used as a tuneable parameter to adjust the depth of the modelled transit. The exact value was not calculated; rather, varying values were used in order to select (by eye) which gave the dip closest to that of the observed transit.

F_b is a measure of the amount of flux blocked by the exoplanet. In order to determine the total flux received by the observer, F_b was subtracted from a value of the off-transit flux. The observed lightcurves have normalised off-transit fluxes, so the total flux recieved over the observation period is just $F_{tot} = 1 - F_b$ for each source.

V. Error Analysis

The signal-to-noise ratio for a given detector observing a source with signal N^* using a number of pixels n_{pix} is given in Howell (2006) and found in Appendix II. The adapted form (equation 8) was used in this project to calculate the total noise from all contributions in a frame.

$$N_{source} = \sqrt{(N^* + N_S) + n_{pix}(N_D + (N_R)^2)} \tag{8}$$

Howell defines the variables as follows: N_S is the number of photons per pixel from the background. Similarly N_D and N_R are the total number of dark current electrons per pixel and the total number of dark current electrons per pixel respectively.

The LCOGT telescope network writes values of dark current and read noise from its CCDs to the .FITS headers produced by them. It also writes the dimensions in both x and y planes of its CCD array, allowing the straightforward calculation of

n_{pix}. Furthermore when analysing the data using photometry, the $(N^* + N_S)$ term is the signal from within the aperture. These values were used to calculate N_{source} for each frame, repeating for any calibration stars considered.

The errors for the transiting system, a calibration star and the background could then be combined to determine the error on equation 5. Partially differentiating equation 5 with respect to all variables and using the quadrature sum nature of error propogation yielded equation 9.

$$\Delta S = \sqrt{\frac{(\Delta N_{source}{}^2)(N_{calib} - N_{source})^2 + (\Delta N_S{}^2)(N_{source} - N_{calib})^2 + (\Delta N_{calib}{}^2)(N_{source} - N_S)^2}{(N_{calib} - N_S)^4}} \tag{9}$$

ΔN_{source}, ΔN_S and ΔN_{calib} are the errors on the source signal, background signal and calibration star signal respectively as calculated using the methods discussed earlier. N_{source}, N_S and N_{calib} are the signals from the source star, the background and the calibration star respectively. The resulting values of ΔS were then plotted as error bars in the y-plane on plots of S as a function of time.

To determine the error for the calculated radius, equation 1 was treated in the same way as seen in equation 10.

$$\Delta R_{exo-obs} = \sqrt{\left(\frac{\Delta F}{F}\right)(\Delta(\Delta F))^2 + \left(\frac{R_{star}{}^2}{4}\right)\left(\frac{F}{\Delta F}\right)(\Delta R_{star})^2 + \left(\frac{R_{star}{}^2}{4}\right)\left(\frac{\Delta F}{F^3}\right)(\Delta(F))^2} \tag{10}$$

The error estimate on the fractional flux blocked, $\Delta(\Delta F)$, was estimated by performing a root mean square analysis on the observed data with respect to the model EPTM curve.

The error on the radius as determined by the EPTM model, $\Delta R_{exo-EPTM}$ was taken to be the difference between lines of best and worst fit that could still fit the data comfortably within the error ranges. These lines were adjusted by eye rather than using an automated scheme. A more rigorous statistical analysis that would use an automated scheme, and therefore be more accurate, would be performed given more time.

IV. Results

I. Practice Data Set: QATAR-1b

After analysing the QATAR-1b dataset using the photometry process defined earlier, figure 6 is the resulting lightcurve. The EPTM model transit is also overlying the observed data. The radii and densitiies determined from the curve can be found in table 3.
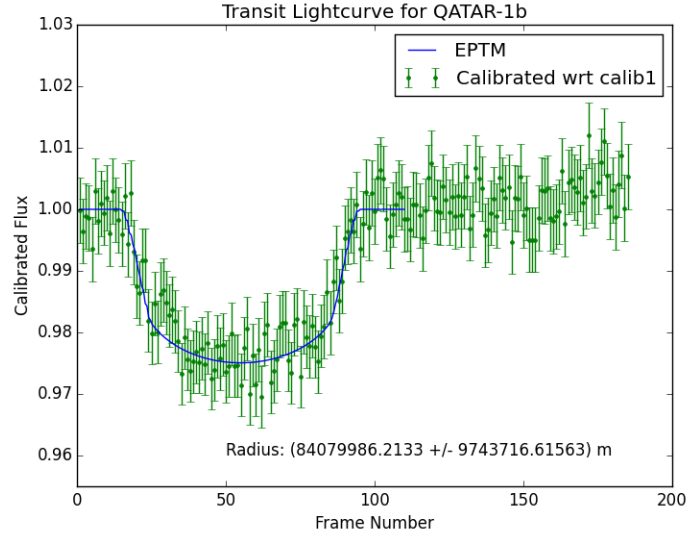
Figure 6: *The resulting lightcurve after analysing the QATAR-1b data using aperture photometry. Overlayed is the theoretical modelled transit using the EPTM code in Appendix I.*

Calculated Radius (m)	EPTM Radius (m)	Known Radius (m)	Calculated Density (kgm^{-3})	Known Density (kgm^{-3})
$(8.41 \pm 0.97)x10^7$	$(9.03 \pm 0.79)x10^7$	$(8.14 \pm 0.3)x10^7$	(832 ± 296)	690^{+98}_{-84}

Table 3: *A table showing numerical values calculated in this project. Both the radius calculated using the dip in the observed lightcurve and the radius calculated using the dip in the EPTM lightcurve are shown, along with the published values for comparison. The same is true of the calculated and published densities.*

The plot shows the characteristic trough as is to be expected from a transit lightcurve. However, there is still some scatter between data points. This is to be expected, as photon arrival at the detector is a random event as described by Poisson statistics.

The EPTM curve fit was performed by eye, and this is reflected in the error values in the radius determined from it in table 3. The scatter, particularly in the trough, made it difficult to estimate the true depth of the transit. A root mean square test could help eliminate this uncertainty and improve the accuracy of the fit, and this is something that could be explored in more detail in future work.

Comparing the values, it can be seen that the calculated radius and EPTM radius are within agreement within their error ranges. The known radius is also within both the calculated radius and EPTM radius error ranges, althrough both the calculated radius and EPTM radius are overstimated. This is attributable to both the difficulty of fitting the curve accurately but also that the transit method gives an upper limit of the mass of the exoplanet. The errors in these instances are both reasonable, though higher than the error on the published value.

The density is is once again overestimated, and the errors here are much larger especially when compared to those of the published values.

II. Observed Data

Regrettably the scheduled data, after anaylsis, didn't show any visible transits. The lightcurves plotted using this method can be seen in figures 7, 8and 9.

Figure 7: *The lightcurve plotted after analysing the data from the observations of WASP-22b. As can be seen, no transit is observed in the lightcurve.*

Figure 8: *The lightcurve plotted after analysing the data from the observatiosn of WASP-78b. This lightcurve shows evidence of a transit, but it was suspected that bad weather obscured the dip.*
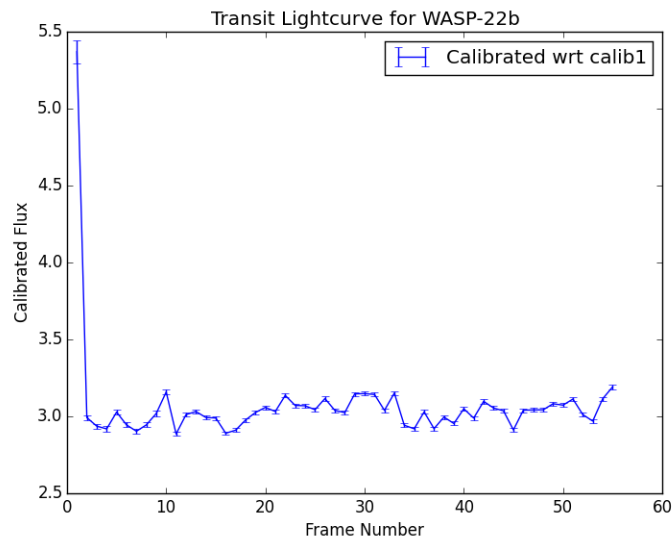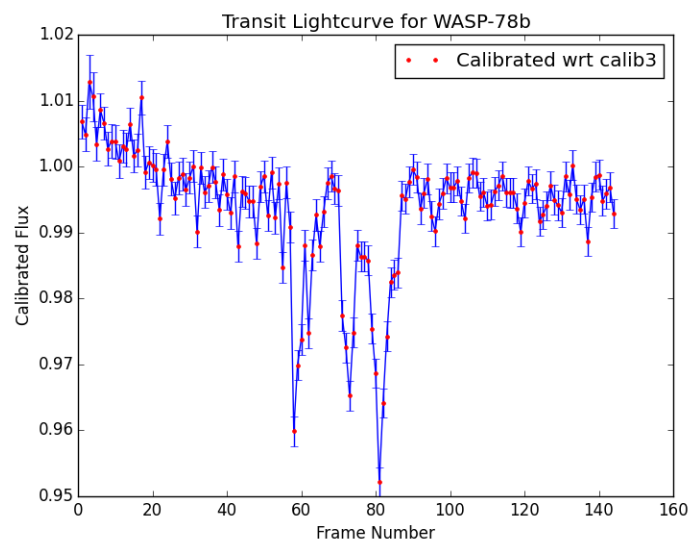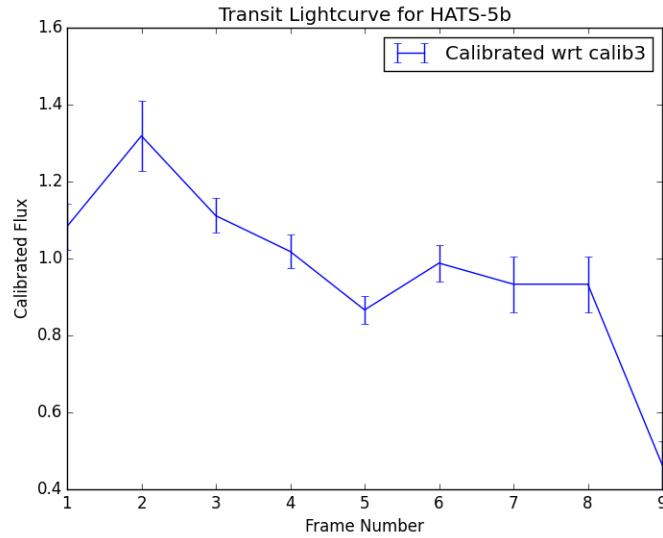
Figure 9: *The lightcurve plotted after analysing the data from the observations of WASP-78b. As can be seen, no transit is observed in the lightcurve.*

Figure 8 showed some evidence of a transit at the point it would be expected (the middle of the observation windoww). This dataset was analysed using the the LEMON differential photometry script (Terron 2015), an automatic script to perform differential photometry and plot lightcurves for a user input folder containing the .FITS files to be anaylsed. Unfortunately the software could not be installed on a Linux machine in time to be analysed, so the data was sent to the software author and the LEMON reduced graphs sent back. They showed the same behaviour and as such it was concluded that bad weather, localised to the portion of sky in which the target system was found, obscured the transit.

The lightcurves in figures 7 and 9 show no evidence of transits. Their .FITS files showed artefacts such as brightening out on the limbs of the images, as well as some flat fielding correction problems. The observing conditions as written to the .FITS headers showed that they were not sufficient to cause these issues.

III.   Known Transiting Datasets

Replacement data sets that contained known transits were provided by Dr. E. L. Gomez. These were analysed using the routines descibed and the lightcurves produced can be seen in figures 10 and 11. The determined quantities can be seen in table 4.

Figure 10: *The lightcurve plotted after analysing the data from the WASP-12b dataset provided by Dr. E. L. Gomez. As can be seen, no transit is clearly visible within the lightcurve. The green datapoints are the photometry reduced data (with errorbars) and the blue line is the EPTM modelled transit.*
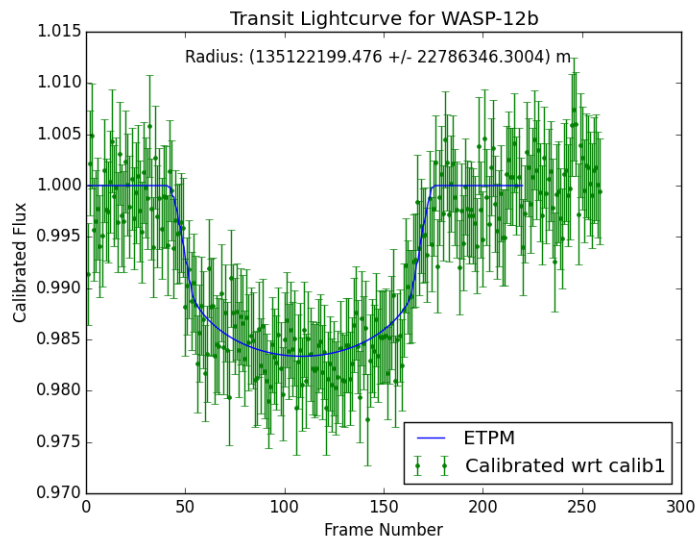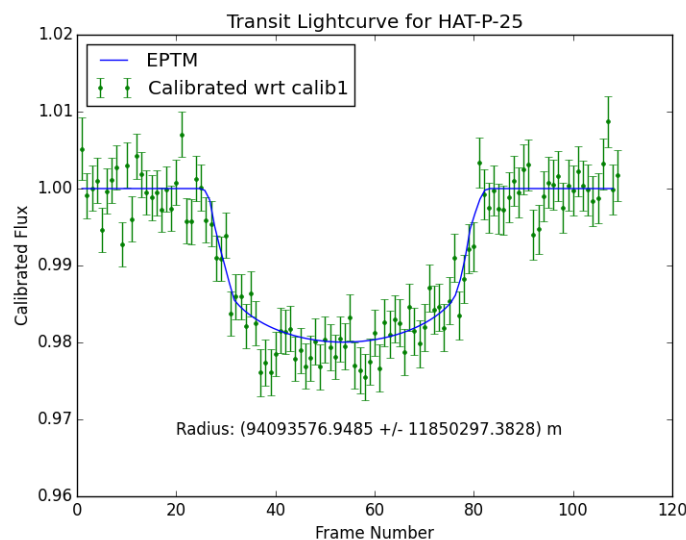

Figure 11: *The lightcurve plotted after analysing the data from the WASP-12b dataset provided by Dr. E. L. Gomez. As can be seen, no transit is clearly visible within the lightcurve. The green datapoints are the photometry reduced data (with errorbars) and the blue line is the EPTM modelled transit.*

Exoplanet	Calculated Radius (m)	EPTM Radius (m)	Known Radius (m)	Calculated Density (kgm^{-3})	Known Density (kgm^{-3})
WASP-12b	$(13.5 \pm 2.2)x10^7$	$(14.3 \pm 1.78)x10^7$	$(12.1 \pm 0.6)x10^7$	(258 ± 132)	240^{+30}_{-20}
HAT-P-25b	$(9.4 \pm 1.2)x10^7$	$(9.42 \pm 1.03)x10^7$	$8.31x10^7$*	(308 ± 110)	420 ± 70

Table 4: *A table showing numerical values calculated in this project for WASP-12b and HAT-P-25b. Both the radius calculated using the dip in the observed lightcurve and the radius calculated using the dip in the EPTM lightcurve are shown, along with the published values for comparison. The same is true of the calculated and published densities. *: no error was quoted in the published result.*

V. Conclusions

VI. Future Work

Bibliography

Addison B. C., Durrance S. T., and Schwieterman E. W. (2010). "Modeling and Observing Extrasolar Planetary Transits". *Journal of the Southeastern Association for Research in Astronomy* 3, pp. 45–51.

Charbonneau D. et al. (2007). "When Extrasolar Planets Transit Their Parent Stars". *Protostars and Planets V*, pp. 701–716. eprint: `astro-ph/0603376`.

Draper P. W. et al. (2014). *GAIA: Graphical Astronomy and Image Analysis Tool*. URL: `http://starlink.jach.hawaii.edu/starlink`.

Einstein A. (1936). "Lens-like action of a star by the deviation of light in the gravitational field". *Science* 84.2188, pp. 506–507.

Extrasolar Planets Encyclopaedia (2014). *Extrasolar Planets Encyclopaedia*. URL: `http://www.exoplanet.eu`.

Haswell C. A. (2010). *Transiting Exoplanets*.

Howell S. B. (2006). *Handbook of CCD Astronomy*. 2nd ed. Cambridge University Press.

Jenness T. et al. (2014). *ORAC-DR: Astronomy data reduction pipeline*. URL: `https://github.com/Starlink/ORAC-DR`.

LCOGT 1-meter Telescope Specifications (2014). URL: `http://lcogt.net/observatory/1m`.

LCOGT Data Pipeline (2012). URL: `http://lcogt.net/observatory/data/pipeline`.

LCOGT Observatory Sites (2014). URL: `http://lcogt.net/observatory/sites`.

Mayor M. and Queloz D. (1995). "A Jupiter-mass companion to a solar-type star". *Nature* 378.1, pp. 355–359.

Morton T. D. and Johnson J. A. (2011). "On the Low False Positive Probabilities of Kepler Planet Candidates". *The Astrophysical Journal* 170.738, pp. 1–12.

NASA Exoplanet Archive (2010). *Transit Example Image*. URL: `http://exoplanetarchive.ipac.caltech.edu/applications/TransitSearch/guide/img/transit.jpg`.

Paddany S., Brat L., and Pejcha O. (2014). *Exoplanet Transit Database*. URL: `http://var2.astro.cz/ETD/`.

Sahu K. C. et al. (2006). "Transiting extrasolar planetary candidates in the Galactic bulge". *Nature* 443.7111, pp. 534–540.

Santerne A. et al. (2013). "Astrophysical false positives in exoplanet transit surveys: why do we need bright stars ?" *ArXiv e-prints*. arXiv: `1310.2133 [astro-ph.EP]`.

Sorensen P., Azzaro M., and Méndez J. (2002). *Object Visibility - STARALT, Isaac Newton Group of Telescopes*. URL: `http://catserver.ing.iac.es/staralt/`.

Sumi T. et al. (2011). "Unbound or distant planetary mass population detected by gravitational microlensing". 473, pp. 349–352. DOI: `10.1038/nature10092`. arXiv: `1105.3544 [astro-ph.EP]`.

Terron V. (2015). *LEMON: differential photometry*.

Townsend R. (2013). *Radial Velocity Image*. URL: `http://www.astro.wisc.edu/~townsend/resource/teaching/diploma/doppler.jpg`.

Udry S. and Santos N. C. (2007). "Statistical Properties of Exoplanets". *The Annual Review of Astronomy and Astrophysics* 45, pp. 397–493.

Van Hamme W. (1993). "New Limb Darkening Coefficients for Modeling Binary Star Light Curves". *The Astronomical Journal* 106.5, pp. 2096–2117.

Wolszszan A. and Frail D. A. (1992). "A planetary system around the millisecond pulsar PSR1257 + 12". *Nature* 355.doi:10.1038/355145, pp. 145–147.

I. Appendix: EPTM Code

```
'''
Project: Exoplanetary Detection and Characterisation
Supervisor: Dr. Edward L Gomez

Author: Tomas James

Script: Prototype for modelling exoplanetary lightcurves
'''

import numpy as np

def model(start, mid, end, nobs, Mstar, Rstar, Mplanet, Rplanet, radius, a, mu, i, sangle):

    '''
    Takes a planetary system consisting of an exoplanet of mass M_planet
    orbiting a star of mass M_star and radius R_star and models a light-
    curve using equations defined in Addison, Durrance and Shwietermann.

    Uses equation 7 in Addison, Durrance and Shwietermann to calculate the
    total flux blocked per pixel solid angle, F_A, of a transiting
    exoplanet.
    '''


    ########################################################################
    ############### List constants and determine basic parameters ##########
    ########################################################################

    # Define constants
    G = 6.673E-11 # Universal gravitational constant
    #m_ref = -1.5 # Apparent magnitude of Sirius
    #I_ref = (40*3.846e26)/(4*np.pi*(9.46e15)**2) # Intensity of Sirius. Units: W/m**2
    # N.B. Above is from I = L/4piR**2 where R = distance from Earth

    # Determine intensity of star (from apparent magnitude equation)
    #I_0 = I_ref*10**((2.5)*(13.19-11.69))
    I_0 = 1


    ########################################################################
    ########## Determine times over which transit has been observed ########
    ########################################################################

    # T is the time between observation start and the transit midpoint
    T = np.linspace(-(mid-start), +(end-mid), nobs)

    ########################################################################
    ############### Compute orbital velocities and angles ##################
    ########################################################################
```

```
# Computes orbital velocity using two masses and the semi major-axis
vorb = np.sqrt(G*(Mstar + Mplanet)/a)

# Determine angular velocity where T = time from transit midpoint (s)
#omega = vorb/a

# Use above to calculate orbital phase angle
#angle = T*omega
#phase = np.linspace(-angle, angle, (nobs+1))


##########################################################################
########### Split exoplanet into arbitrary number of pixels ############
##########################################################################

# Generates arbitrary coordinates in pixels and finds those that fit
# within radius**2 (i.e. pythagorean). This is then used to calculate
# these values as a fraction of the exoplanet radius.
'''
for x, y in product(np.linspace(-radius, radius, npix), repeat=2):
    if x ** 2 + y ** 2 <= radius**2:
        x_coord.append((x/radius)*Rplanet)
        y_coord.append((y/radius)*Rplanet)

# Converts above lists to arrays for compatibility purposes
x_coord = np.asarray(x_coord)
y_coord = np.asarray(y_coord)
'''

# Generates arrays of coordinates in x and y planes from -radius
# to +radius with 2radius+1 points
x = np.linspace(-radius, +radius, (2*radius+1))
y = np.linspace(-radius, +radius, (2*radius+1))

# Tiles these 2 arrays into cartesian coordinate pairs
coords = np.transpose([np.tile(x, len(y-1)), np.repeat(y, len(x-1))])

# Splits that 2d array into 1d arrays of all x and y points. This
# differs from x and y by being the (x,y) coordinates of each pair,
# whereas x and y is just the dimension of each plane.
x_coord = coords[:,0]
y_coord = coords[:,1]

# Creates list to house values iterated through to see if they lie
# within the exoplanet
x_exo, y_exo = [], []

# Loops through all pair coordinates to determine if the coordinate
# lies within radius**2 (Pythagorean). If it does it is appended to
# the list above to create an array of coordinates that are within
# the exoplanet.
for i in range(len(coords)):
```

```python
        if x_coord[i]**2 + y_coord[i]**2 <= radius**2:
            x_exo.append((x_coord[i]/radius)*Rplanet)
            y_exo.append((y_coord[i]/radius)*Rplanet)

    # Converts above lists to arrays for compatibility purposes
    x_exo = np.asarray(x_exo)
    y_exo = np.asarray(y_exo)

    print x_exo*(radius/Rplanet)
    print y_exo*(radius/Rplanet)



    ############################################################################
    ################## Compute positions relative to star ##################
    ############################################################################

    # Declare array to house values of x and y position
    X_pos = np.zeros(len(T))
    #Y_pos = np.zeros(len(phase))

    # Determine values of x position
    X_pos = vorb*T

    # Declare array to house flux values
    F_A = np.zeros(len(X_pos))

    # Determine y position (distance perpendicular to x position)
    #Y_pos = a*(np.arcsin(2*np.pi - radians(i)))
    #Y_pos = a*(np.sin(np.radians(i)))
    Y_pos = 0

    # Declare array to house distances from centre of star
    #dpix = np.zeros((len(X_pos)))



    ############################################################################
    ############### Determine flux blocked per pixel solid angle #############
    ############################################################################

    # Determine position (postion from transit midpoint across stellar disk)
    for i in range(len(X_pos)):
        F_block = 0
        count = 0
        for j in range(len(x_exo)):

            #X_pos[i] = a*np.sin((phase[i]))
            #X_pos[i] = vorb*T[i]

            # Determine distance between centre of planetary disk and stellar disk
            # The numpy.sqrt allows sqrt of an array
            dpix_a = np.sqrt(((X_pos[i] + x_exo[j])**2) + (Y_pos + y_exo[j])**2)
```

```python
        # Loop over intervals of d to calculate flux blocked. If the distance
        # to the exoplanet lies within the radius of the star, the flux blocked
        # is calculated using equation 7 of A, D and S paper.
        # If it lies outside of the radius of the star, the flux blocked is assigned
        # a 0 value (as is in the array anyway).
        if dpix_a <= Rstar:
            count += 1

            F_block += (I_0*(1-mu*(1-np.sqrt(1-(dpix_a/Rstar)**2))))/len(x_exo))*sangle

    F_A[i] = F_block


#########################################################################
################## Determines the lightcurve values ####################
#########################################################################

# Use simplified form of equation 7 to determine off-transit flux
#F = np.ones(len(X_pos))*(I_0*(1-mu))
F = np.ones(len(X_pos))

# Subtract flux blocked from F to determine total flux per unit pixel solid angle
tot_F = F - F_A

#########################################################################
######################### Compute parameters ###########################
#########################################################################

# Determine fractional change in flux
delta_F = max(F_A)

# The fractional change in flux is proportional to the sqaure of the radius
# of the exoplanet divided by the square of the stellar radius.

det_Rplanet = np.sqrt((Rstar**2)*(delta_F/F[0]))

print '\n The estimated radius of the exoplanet is', det_Rplanet, 'm. \n'

return tot_F, X_pos, T, det_Rplanet
```